APS physics

CHORUS

This is the accepted manuscript made available via CHORUS. The article has been published as:

Depth resolved granular transport driven by shearing fluid flow

Benjamin Allen and Arshad Kudrolli

Phys. Rev. Fluids **2**, 024304 — Published 28 February 2017

DOI: 10.1103/PhysRevFluids.2.024304

Depth resolved granular transport driven by shearing fluid flow

Benjamin Allen and Arshad Kudrolli

Department of Physics, Clark University, Worcester, MA 01610

(Dated: September 30, 2016)

Abstract

We investigate granular transport by a fluid flow under steady state driving conditions, from the bed-load to the suspension regime, with an experimental system based on a conical rheometer. The mean granular volume fraction ϕ_g, the mean granular velocity u_g, and the fluid velocity u_f are obtained as a function of depth inside the bed using refractive index matching and particle tracking techniques. A torque sensor is utilized to measure the applied shear stress to complement estimates obtained from measured strain rates high above the bed where $\phi_g \approx 0$. The flow is found to be transitional at the onset of transport and the shear stress required to transport grains rises sharply as grains are increasingly entrained by the fluid flow. A significant slip velocity between the fluid and the granular phase is observed at the bed surface before the onset of transport as well as in the bed-load transport regime. We show that u_g decays exponentially deep into the bed for $\phi_g > 0.45$ with a decay constant which is described by a nonlocal rheology model of granular flow that neglects fluid stress. Further, we show that u_f and u_g can be described using the applied shear stress and the Krieger-Dougherty model for the effective viscosity in the suspension regime where $0 < \phi_g < 0.45$, and where $u_g \approx u_f$.

I. INTRODUCTION

The dynamics of a horizontal granular bed under the action of a fluid flow is an important model to understand a wide range of problems, from sediment transport in streams and fractures, to the fluid mediated delivery of powders and grains in various medical and engineering applications. In the slow flowing bed-load regime, grains are considered to move over the surface while maintaining contact with the bed surface over a significant fraction of the time [1, 2]. In the fast moving suspension regime, grains can be carried by the fluid for long periods of time. While there have been a number of studies which have examined the onset of motion and the net granular flux as a function of driving conditions and grain properties [3–7], the nature of the granular flux and the fluid flow as a function of depth remains unresolved. This is because granular materials are typically opaque and it is difficult to measure their packing properties and dynamics in the dense regions inside the bed. Furthermore, numerical simulations have been developed [8–12], but remain challenging, because of the multiple scales involved in simulating grain-fluid interactions.

Recently, experiments have been developed with transparent beads which can be index matched using appropriate fluids to examine the bed structure and dynamics away from the direct influence of side walls [6, 13–15] to go beyond studies in horizontal and inclined quasi-two dimensional beds which were visualized through the side walls [16, 17]. Most of these studies have been conducted with acrylic beads which have densities similar to the shearing fluid, and have been performed in the viscous limit. Some of these studies have reported that the granular flow is confined to a moving layer in which the velocity decays quadratically to zero at a depth which scales linearly with applied shear stress [13]. Two-phase models combining Coulomb friction and linear drag, and its variations have been proposed [13, 14] to explain the observed trends assuming that fluid velocity and granular velocity are approximately equal inside the bed in a region where the granular volume fraction and the effective viscosity of the fluid can be also assumed to be relatively constant. However, a critical examination of the reported trends and comparisons reveals systematic deviations that are further highlighted by the report of creeping granular flows in a similar system [15]. Numerical simulations using coupled Discrete Element Method have been used to investigate the granular rheology in bedload transport [12], and appear to suggest that the inertial number dependent friction rheology developed in the case of dry

granular materials [18], can be used to describe the rheology of the bed in the dense granular flow regime but not in the less dense layers above. Furthermore, the depth resolved transport has not been reported in cases where the relative density of the grains is significantly higher than the fluid, as in natural sand. The strength of the flow required to transport grains can be expected to be higher under these circumstances, and thus it is possible that the flow can be beyond the viscous regime when onset is reached. Thus, a satisfactory description of the spatial distribution of granular transport is still lacking, and further studies are needed to develop a description of the observed trends using appropriate constitutive laws.

In this paper, we report an investigation of a granular bed sheared by a fluid flow with a novel experimental system in which a bed of glass beads immersed in a fluid is sheared by means of a rotating conical top surface. We obtain the depth resolved packing fraction and velocity of the grains and fluid inside the bed, using refractive index matching techniques, from well below to well above onset of transport under steady state conditions. We deduce the applied shear stress from the measured shear rate of the clear fluid phase well above the bed surface where grains are absent. Further, we also obtain the applied shear stress as a function of rotation rate by measuring the torque applied on the container. We compare and contrast the applied shear stress in case of a granular bed and a solid planar substrate to understand the flow regime and the relative contribution of viscous and inertial forces in the system. The onset of transport is found to occur in the transitional regime between laminar and turbulent. When the driving is increased above onset, bed-load transport and bed creep are observed to occur with a growing suspension phase developing as the driving is increased further. We find that the mean velocity of the grains decay exponentially into the bed and can be scaled onto a single curve by using the velocity corresponding to a depth where the granular fraction is 75% of the maximum value. We show that the velocity profile in this dense regime is similar to the velocity profile observed in boundary sheared granular beds in gravity, where fluid effects are negligible. Further, we show that mean grain velocity in the suspension regime can be described using the Krieger-Dougherty model [19] for the effective viscosity of suspensions as a function of grain volume fraction, provided the mean grain and fluid velocities are similar.

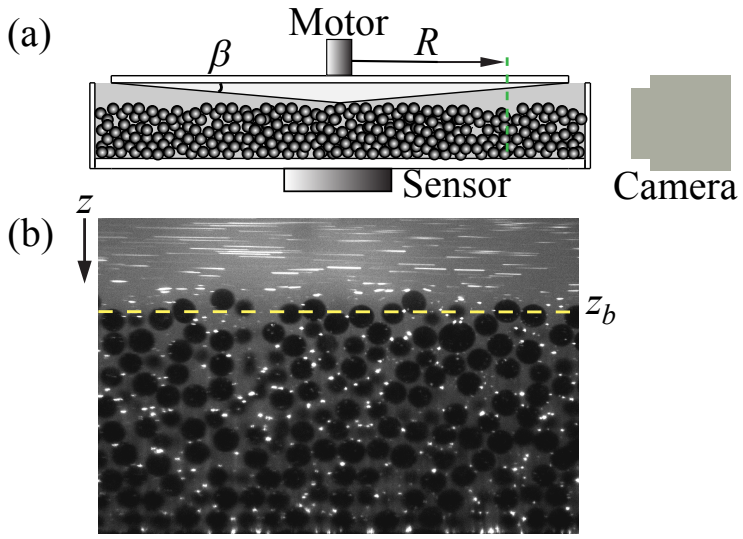


FIG. 1. (a) A side view of the schematic of the experimental apparatus. The conical top plate is rotated about its axis with an angular frequency f. A laser sheet (dashed vertical line) illuminates the fluorescent dye and the fluorescent tracers in the fluid. The applied torque is measured with a torsional sensor on which the container rests. (b) A sample image showing grains which appear dark in contrast with the fluid which appears gray and tracers which appear white. z_b indicates the average depth below which $\phi_g > 0.45$.

II. EXPERIMENTAL SYSTEM AND PROTOCOLS

The experimental apparatus is shown in Fig. 1(a) and consists of a circular glass container with inner radius $R_c = 95\,\mathrm{mm}$ and with a textured bottom with roughness $k = 0.5\,\mathrm{mm}$. The container is filled with a fluid with density $\rho_f = 1002\,\mathrm{kg\,m^{-3}}$ and kinematic viscosity $\nu = 0.021\,\mathrm{Pa\,s}$. Approximately 1.5×10^5 glass beads with density $\rho_g = 2500\,\mathrm{kg\,m^{-3}}$ and diameter $d = 1.05 \pm 0.05\,\mathrm{mm}$ are added in a 9 mm deep flat layer. Thus, the relative density ρ_g/ρ_f is similar to typical sediment flow systems [3]. The roughness of the container bottom prevents the grains from sliding easily on the substrate, confining the studied movement to the interaction of the fluid with the individual granules of the bed. A plate with a conical surface, which makes an angle $\beta = 5^o$ with the horizontal, is then lowered into the container so that its apex coincides with the top of the horizontal granular bed. The linear increase in the height of the top plate compensates for the fact that its tangential velocity increases linearly with distance from the axis of rotation resulting in uniform shear in the case of a solid flat substrate. The top plate is rotated by a motor with prescribed frequencies f up to 3 Hz to then shear the fluid under steady state conditions.

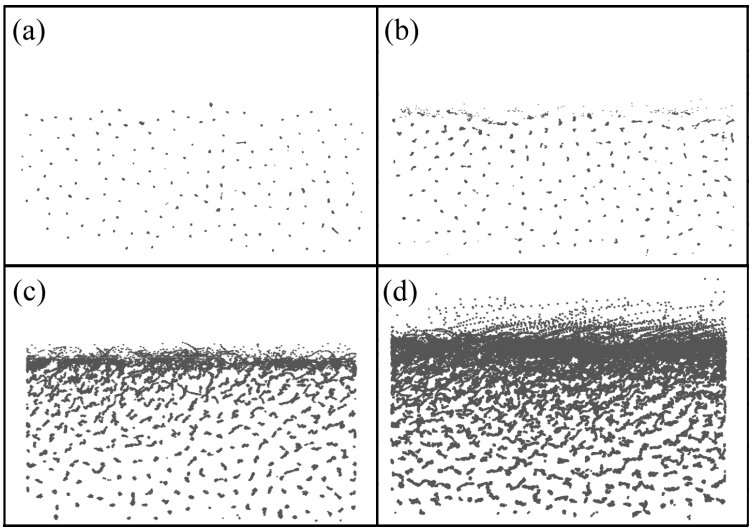


FIG. 2. The positions of grains tracked over 1000 frames acquired at 60.1 fps (a) $f/f_c = 0.37$, (b) $f/f_c = 1.04$, (c) $f/f_c = 1.26$, and (d) $f/f_c = 1.33$. The grains appear stationary in the case of $f/f_c = 0.37$ to within the errors in determining their centers. Grains are observed to move significantly near the surface in the case of $f/f_c = 1.04$ and $f/f_c = 1.26$, with creep motion deeper in the bed. Grains moving over smooth arcs that are well over a grain scale can be observed near the surface in the case of $f/f_c = 1.33$ indicating the development of a suspension regime near the top of the bed.

The refractive index of glass beads and the fluid are matched to within 0.01% and a fluorescent dye and fluorescent tracer particles with diameter 15 μm are added to the fluid to visualize the system. A vertical cross section of the system is then illuminated with a 532 nm wavelength laser in a $0.2d$ thick plane to contrast the glass beads and the fluid [20]. We image a plane at a distance of $R/R_c = 0.78$ from the axis of rotation to minimize side wall effects while allowing the mean flow to be approximated as being planar within 1% over the viewing window.

Fig. 1(b) shows an image taken with a 10 ms exposure using a high quantum efficiency Hamamatshu ORCA-Flash 4.0 LT camera placed orthogonal to the illumination plane. The grains appear relatively dark, while the tracer particles appear as bright dots or short streaks depending on the fluid speed. We filter the image to remove the bright pixels due to the tracers, and identify grains with cross sections which are at least $0.65d$ in diameter in the image plane. The centers are found to within $\pm 0.1d$ using the centroid of the dark pixels corresponding to the grain. In order to obtain the fluid velocity, we use Particle Image Velocimetry (PIV) with images acquired at 0.1 – 500 fps in regions where the fluid velocities are less than 60 cm s^{-1}. We further complement the fluid velocity data in faster flowing

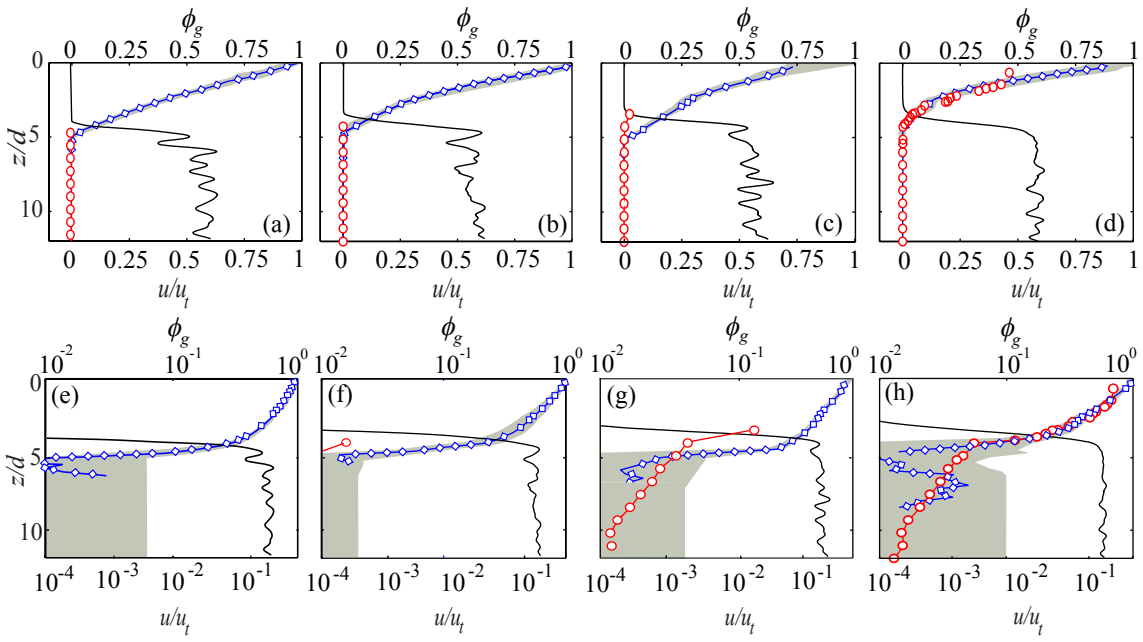


FIG. 3. The volume fraction ϕ_g (—) and grain velocity normalized by the top plate velocity $u_g(z)/u_t$ (-○-) and fluid velocity normalized by the top plate velocity $u_f(z)/u_t$ (-◇-) as a function of depth for (a) $f/f_c = 0.37$, (b) $f/f_c = 1.04$, (c) $f/f_c = 1.26$, and (d) $f/f_c = 1.33$. The root mean square fluctuations in $u_f(z)/u_t$ are noted in gray. (e-h) The data is plotted in log-linear scale to capture the wide variation observed in ϕ_g, u_g, and u_f. The range of errors are indicated by the shaded gray areas.

regions by measuring the streak length made by the tracers over a given exposure time, as well as by particle tracking inside the bed where the tracers do not move significantly over the duration of the recording. The volume fraction of the grain ϕ_g is obtained from the image average intensity measured as a function of depth z from the top plate, and mapping it to a known volume fraction of the grains [21].

III. MEASUREMENTS

We initialize the bed by rotating the top plate at $f = 3\,\mathrm{Hz}$ for thirty seconds to fully suspend the grains in the fluid and then stopping the rotation suddenly. This protocol is found to result in a uniformly sedimented bed with a horizontal surface. Then, by increasing the rotation frequency in small increments and waiting for any transient motion to decay, we determine sustained granular transport to occur above $f_c = 1.35 \pm 0.05\,\mathrm{Hz}$. Transient motion was observed to occur well below onset, with grains rearranging and settling in place over a scale of less than a grain size. A few grains at the surface were also observed to move

over a significant distance before redepositing back on the surface. However, this motion was not observed to lead to sustained transport of the bed for $f < f_c$ with all activity ceasing given sufficient time under steady state driving. The transient time was observed to increase as f_c was approached, similar to previous observations in a linear pipe geometry [7], and thus f_c can be interpreted as the driving parameter where the decay time scale has diverged. Furthermore, f_c was observed to be history-independent with the same range of values observed whether the bed was resuspended or not between each increment of f.

The position of the grains inside the bed, recorded over 1000 frames acquired at 60.1 frames per second (fps), are shown in Fig. 2(a-d) at various rotation frequencies from well below to above onset of transport under steady state conditions. In the case of $f/f_c = 0.37$, one finds that the identified positions of the grains overlap to within the error in finding the centers, showing that the grains are stationary over the recorded duration. (We further tested that the grains appear stationary when examined over a day under the same conditions.) Just above onset at $f/f_c = 1.04$, one observes that the grains near the bed surface move by apparently rolling at the surface consistent with the description of bed-load transport [2]. The grains at the surface are fully mobile at higher $f/f_c = 1.26$, and yet appear to be in contact with the bed because any arcs of points at the surface appear to be of order of the grain size, and thus indicative of bed-load transport. As f/f_c is increased to 1.33, grain positions describing arcs over several grain lengths become evident at the surface, indicating the development of a suspension phase. The grains deep into the bed are clearly observed to be mobile as the scatter of points appears extended along the flow direction with considerable fluctuations in the vertical direction as the grains rearrange and move in relation to each other.

To quantify the granular packing and dynamics, we plot ϕ_g averaged in horizontal layers of thickness $0.012d$ as a function of depth z from the top plate in Fig. 3. In plotting ϕ_g in log scale, we have plotted the data starting from 0.01 as this represents the noise floor in determining ϕ_g. We observe that ϕ_g increases sharply and fluctuates around a packing fraction $\phi_g \approx 0.60$ into the bed in all cases. This packing is well below the maximum packing of spheres which is 0.74, as well as the maximum random packing of spheres which is approximately 0.64, but comparable to that observed in previous studies of frictional glass sphere packings before application of significant shear [21]. Examining the change in ϕ_g with z across the examples shown in Fig. 3, one observes that the bed interface is

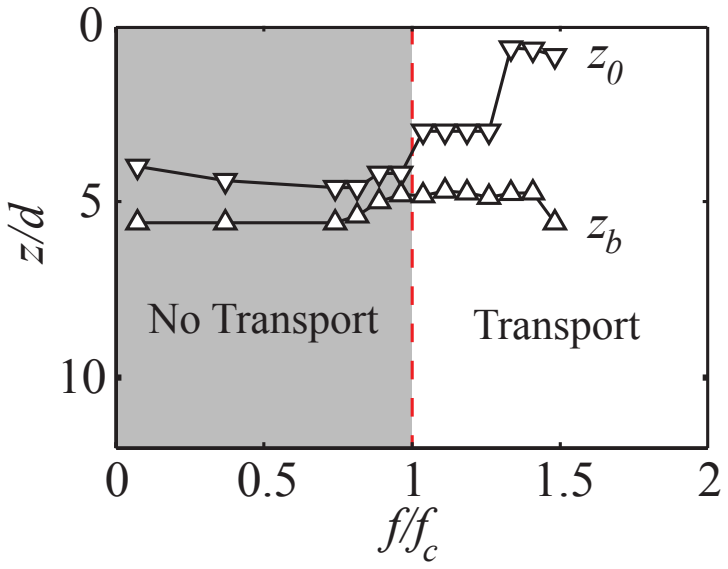


FIG. 4. The measured depth $z_o = z|_{\phi_g=0}$ and $z_b = z|_{\phi_g=0.45}$ denoting the thickness of the bed interface as a function of f/f_c. The error in determing the depths is less than the symbol size. z_o can be observed to increase by a grain diameter at the onset of transport, and further increase to the top of the container when grains are entrained rapidly into suspension at $f/f_o \approx 1.25$.

sharper in the case of $f/f_c = 1.04$ compared with $f/f_c = 0.37$. This is consistent with our earlier observation that grains dislodge and again lodge on the surface as $f \to f_c$. In Fig. 4, we further plot the depth z_o and z_b corresponding to the depth where $\phi_g > 0$, and $\phi_g > 0.45$, respectively over the entire range of f/f_c investigated. The relative sharpening of the interface indicates that the grains which are relatively more exposed to the flow are preferentially dislodged. These grains are then deposited in deeper pockets at the interface, leading to a decreasing surface roughness as $f \to f_c$, before increasing again above the onset of transport. As f/f_c is increased further, ϕ_g decreases to zero at a relatively smaller depth as the suspension phase grows. From Fig. 4, we observe that the dilation of the bed is relatively small. Nonetheless, the increasing entrainment of even a small number of the grains is observed to have a significant effect on the fluid flow as we discuss next.

We then obtain the magnitude of the horizontal component of the mean grain velocity u_g and the fluid velocity u_f normalized by the top plate tangential velocity $u_t = 2\pi f R$ and plot it along with ϕ_g in Fig. 3. Because of the wide range of velocities observed, we have included both a linear-linear plot and a log-linear plot of the u_g and u_f as a function of z. In the case of $f/f_c = 0.37$, where the bed is immobile and $u_g/u_t = 0$, we observe that u_f decreases linearly from the top plate and then decays rapidly over 3 orders of magnitude near the

bed surface over the scale of grain diameter consistent with previous studies of fluid flow near granular interfaces by Golharzadeh, et al [22]. In the case of $f/f_c = 1.04$, u_f appears to decrease non-linearly with z. Then the local shear rate of the fluid $\dot{\gamma}_f = du_f/dz$ can be observed from Fig. 3(b) to be greater near the top plate compared to near the bed surface. We also observe that the difference between $\dot{\gamma}_f$ at the top and at the bed surface grows with f/f_c. Comparing u_f and u_g, we observe a significant slip between the fluid and the granular phase at the bed interface, expect well above onset of transport (see Fig. 3(a-c)). However, u_f and u_g appear to approach each other in the fast moving regions at higher f/f_c (see Fig. 3(d)).

IV. ANALYSIS

A. Reynolds Numbers

To understand the flow regime, we estimate the flow Reynolds number $Re_f = \rho_f UL/\nu$ using the characteristic flow speed $U = 2\pi fR$ and the measured depth of the fluid layer z_b as the size scale L. The observed Re_f is plotted in Fig. 5(a) as a function of f/f_c, and ranges approximately from 30 to 80 for $0.5 < f/f_c < 1.5$. This range of Re_f implies that the flow is transitional over the range of f where grains are transported. Thus, inertial effects can be important to determining the flow. We also estimated the particle Reynolds Number Re_p, which is often used to characterize the flow regime relevant for erosion [5]. Using the measured u_f at the bed surface where $\phi_g = 0.45$ and $L = d$, we find Re_p to be less than 0.1 over the entire range of f/f_c investigated.

B. Applied shear stress

We now relate the experimental driving parameter f to the shear stress acting on the bed using two complementary experimental methods. In one method, we use the measured u_f as a function of z as a result of the motion of the top plate, to estimate the shear stress τ well above the bed in the clear region where the stress-strain relation may be given by viscosity of the fluid. In this case, $\tau = \nu\dot{\gamma}_o$, where $\dot{\gamma}_o$ is the shear rate measured up to depth z_o where $\phi_g = 0$ as shown in Fig. 4. Then one notes that τ along the flow direction is constant with z under steady state conditions. Using the normal stress due the buoyancy subtracted weight

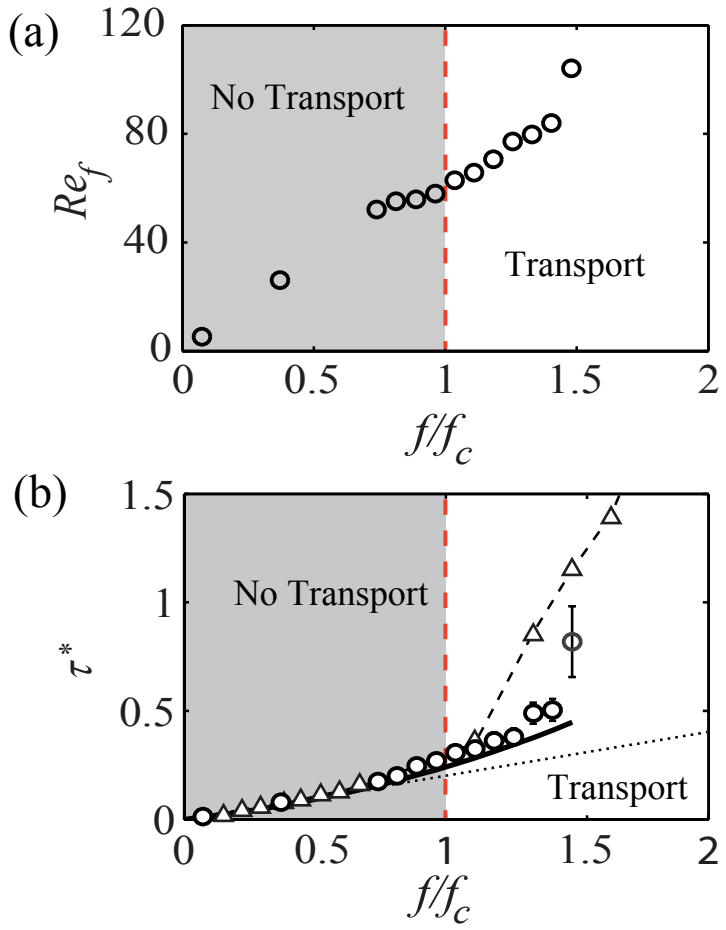


FIG. 5. (a) The flow Reynolds number Re_f shows that the system is in the transitional regime at onset of transport indicated by the vertical dashed line. (b) The non-dimensional shear stress τ^* obtained from measured strain rates $\dot{\gamma}_o$ ($\circ$) increases rapidly above onset of transport. τ^* obtained using torque measurements is plotted with dashed line and triangle symbols (-$\triangle$-). The torque measurement errors are smaller than the symbol size and thus not plotted. τ^* measured from the torque in a flat container with no grains is plotted with solid line (—), and $\tau^* = \nu\dot{\gamma}/\sigma_g$ with $\dot{\gamma} = 2\pi f/\tan\beta$ assuming viscous flow and a flat solid substrate with dotted line ($\cdots$).

of the grains $\sigma_g = (\rho_g - \rho_f)gd$, where g is the acceleration due to gravity, as a relevant scale, we then deduce a non-dimensional shear stress, also known as the Shields Number, acting in the horizontal direction $\tau^* = \tau/\sigma_g$.

Fig. 5(b) shows a plot of τ^* as a function of f/f_c. It can be observed that τ^* increases linearly at first before increasing more rapidly above the onset of transport. To understand the observed τ^* in relation to that for a uniformly sheared fluid in the conical geometry, we also plot $\tau^* = \nu\dot{\gamma}/\sigma_g$, where $\dot{\gamma} = 2\pi f/\tan\beta$. We observe that the initial increase in τ^* agrees with this estimate, before systematic deviations set in at higher f/f_c. These deviations can

occur because of the inertial effects in the flow as indicated by the estimate of Re_f over the same range of f. However, it is also possible to interpret the increase in τ^* as occurring due to an effective increase of viscosity due to an increasing concentration of grains in suspension. Then, a higher shear stress would be required to maintain similar strain rates.

To further check this interpretation and the robustness of the estimated shear stress, we next performed measurement of torque T exerted by the rotating plate using a second complementary method. Here, assuming a constant shear stress τ_T as a function of distance from the rotation axis, one can integrate τ_T along the radius to obtain a relation between the applied shear stress and torque. Inverting this relation, we can express τ_T in terms of T, i.e. $\tau_T = 3T/2\pi R_c^3$. Accordingly, we plot $\tau^* = \tau_T/\sigma_g$ corresponding to a granular substrate in Fig. 5(b). The error bars associated with the measurement are smaller than the symbol size, and significantly smaller compared to the errors which start building up in obtaining τ^* from the strain rate measurements due to particle tracking errors at high speeds. For this reason, we are able to present the data corresponding to the torque up to higher f/f_c. We further plot τ^* obtained from torque measurements as well as for a flat solid substrate to understand the trends associated with the fluid alone.

We observe that τ^* obtained using both methods in all cases overlap at low f/f_c with the viscous limit. Further, systematic deviations start to develop from the linear trend at higher f/f_c which are similar whether using the torque or the direct strain rate methods for estimating τ^*. One can observe that τ^* in the case of the flat substrate also follows the deviations from the linear trend as in the granular case showing that the initial deviation from linearity occurs due to the growth of inertial effects in the fluid flow. At still higher f/f_c, τ^* both increase rapidly well above the trend in the case of solid substrate.

While, the rapid increases τ^* using the two methods do not completely coincide, it is noteworthy that they are within an order of magnitude of each other. The discrepancy likely arises because the assumption that the shear stress is uniform with R in estimating τ^* from the torque measurement fails systematically above the onset of transport, as the moving layer gets deeper. Nonetheless, the rapid increase of τ^* can be interpreted as arising due to an increase in volume fraction of grains in the suspension phase which can lead to an effective increase in its viscosity [23].

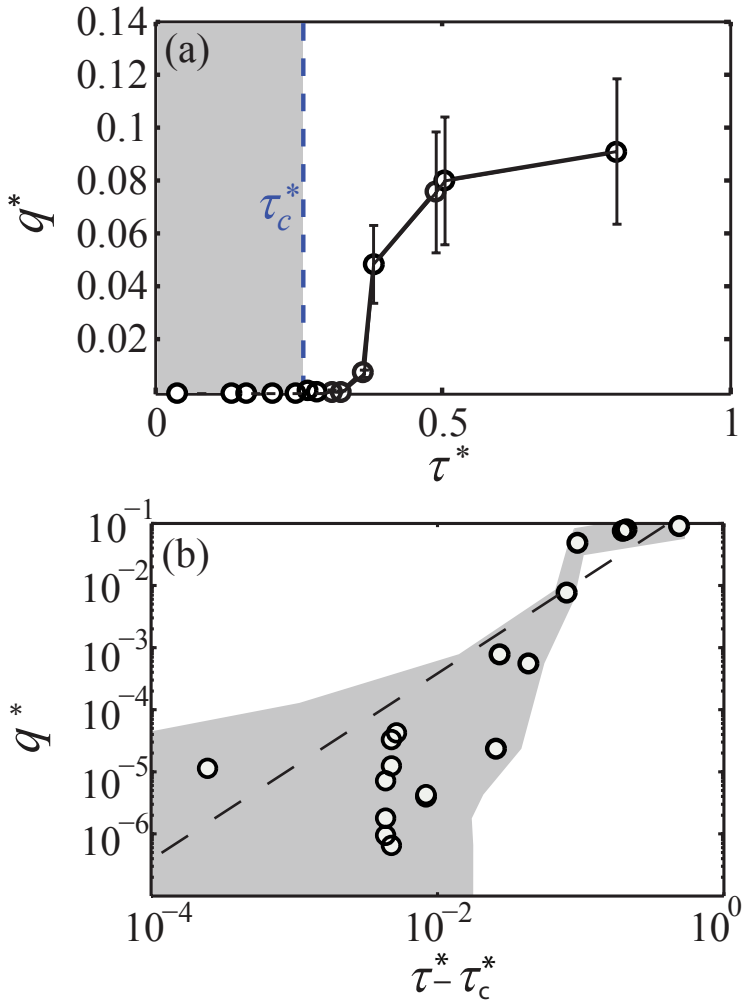


FIG. 6. (a) Non-dimensional Einstein flux q^* as a function of τ^* is observed to increase rapidly over four orders of magnitude above the onset of transport. The vertical dashed line corresponds to τ_c^*. (b) Non-dimensional Einstein flux q^* as a function of $\tau^* - \tau_c^*$, where the critical Shields number τ^* above $\tau_c^* = 0.242 \pm .018$. The dashed line with slope 3/2 corresponds to the Meyer-Peter and Müller law [4]. The area shaded in gray correspond to the error in determing the flux and the shear stress..

C. Critical Shields Number and Granular flux

We now examine the development of granular transport as a function of τ^*. We use τ^* obtained using the strain rate measurements in the following as it is a better measure compared with τ^* obtained using the torque as outlined above. The measured granular mass flux is obtained by integrating the product of the granular volume fraction ϕ_g and the mean granular velocity u_g as a function of depth. This flux is scaled by $\sqrt{(\rho_g/\rho_f - 1)gd^3}$ to give

the Einstein flux [4]

$$q^* = \frac{\int \phi_g(z) u_z(z)\, \mathrm{d}z}{\sqrt{(\rho_g/\rho_f - 1) g d^3}}\,.$$

The error in determing q^* increase with flux because of the difficulty in tracking particles at high speed. This affects the measurement of the speed as well as the volume fraction, both of which contribute significantly to the errors in determining the flux. Fig. 6 shows a plot of q^* as a function of τ^* along with associated error in determining q^*. The flux is measured to rise rapidly as τ^* increases above the critical value $\tau_c^* = 0.242 \pm .018$, and then more slowly at higher τ^* as the suspension phase develops. This measured critical value is within the range of values given by the empirical Shields curve which characterizes the trend observed in the critical Shields number versus the particle Reynolds number data reported in the literature based on measurements in flumes and in the field [3]. Furthermore, the reported value is consistent with our group's previous observations with a different system but with similar sized glass grains [7]. In that study, conducted with a bed of glass grains inside an enclosed linear flume with a rectangular cross section, the critical Shields number was found to increase systematically as the bed was sheared over prolonged periods. Because the critical Shields number in the current study is obtained after steady state conditions are established, we observe that the observed value is consistent within experimental error with the armoured value observed in that system.

To further characterize the rapid increase in granular transport, we plot q^* as a function of the excess stress $\tau^* - \tau_c^*$ in Fig. 6(b). A dashed line corresponding the Meyer-Peter and Müller law in which $q^* \propto (\tau^* - \tau_c^*)^{3/2}$ is also plotted to guide the eye. While the flux is observed to range over many orders of magnitude, a clear scaling is difficult to obtain because the error in determining the flux is significant. Nonetheless, the data is observed to be roughly consistent with that trend within errors of the measurements. We found it impractical to take still longer imaging data sets to reduce the error because it quickly overwhelmed our image storage and processing capacity. Therefore, we do not focus on the scaling of the granular flux in the following but rather on the depth dependent flow profiles as a means to understanding the transport.

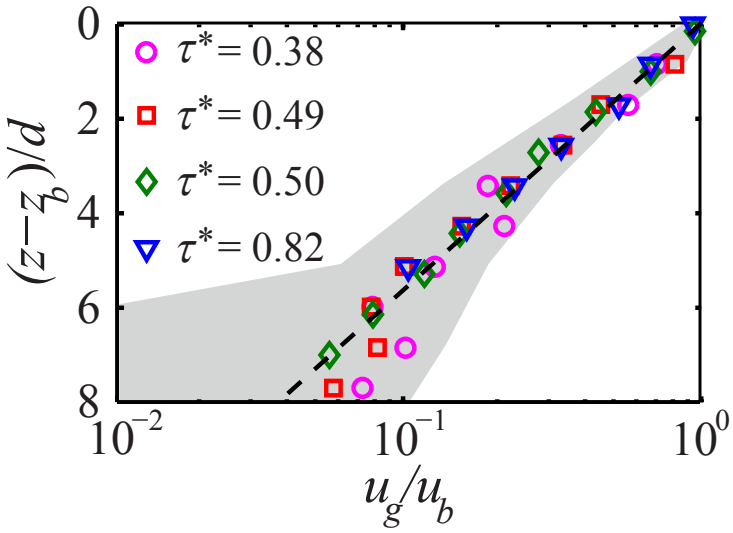


FIG. 7. The grain velocity u_g/u_b as a function of depth $z - z_b$ corresponding to the region where $\phi > 0.45$. u_b is the granular speed at the top of the bed where $z_b = z|_{\phi=0.45}$. The data is described by the dashed line given by Eq. 1. This form is described by a secondary rheology model of a horizontally sheared granular bed which considers the fluid stress to be negligible in determining the velocity profiles [24]. The area shaded in gray correspond to the error in determing the velocities.

V. ANALYSIS OF VELOCITY PROFILES WITH DEPTH

With the above discussion of the relative importance of fluid viscosity, fluid inertia, and entrainment of grains as a function τ^*, we now develop a description of the velocity profiles observed in the experiments based on the rheology of the material.

A. Dense deep flow regime

We first focus on the slow flowing region $z > z_b$ where $\phi_g \geq 0.45$. As noted in the introduction, this region has been described by using a model which incorporates Coulomb friction and drag forces which predicts a quadratic velocity decay into the bed [13]. However, from Fig. 2(g,h), one notes that u_g appears to decay exponentially into the bed in this region. Indeed, exponential decay of granular motion across shear bands are commonly noted in dry as well as submerged granular flows [15, 20, 25, 26].

We plot $(z - z_b)/d$ versus $u_g(z)$ normalized by the velocity observed at z_b in Fig. 7(a) for $\tau^* = 0.35, 0.49, 0.5$, and 0.82 where the flow could be measured over an appreciable depth. All four data sets in this regime are observed to collapse onto a single line corresponding to

an exponential decay. Fitting the data to the function

$$u_g(z)/u_b = \exp\left(-\frac{(z-z_b)}{\delta}\right), \text{ for } z > z_b \tag{1}$$

we find the decay constant $\delta/d = 2.5 \pm 0.1$. This functional form of velocity decay into the bed with the same decay constant was found previously in horizontally sheared granular materials in gravity [20]. Those experiments were performed in the quasi-static limit where the fluid was measured to not have any effect on the effective friction. Thus, the time scale over which grains move past each other, because of shear, is much longer compared to the time scale for the grains to come in contact by draining fluids near grain contacts.

Furthermore, those measured velocity profiles and decay were described more recently by a nonlocal rheology model which incorporates the scale of the grain in predicting the decay of the velocity from a sheared wall [24]. In this model, the flow in a region is affected not only by the local granular stress, but also by the flow in the neighboring regions giving rise to the exponential behavior shown in Fig. 7. Thus, we conclude that the functional form of the creep flow into the bed in the region $z > z_b$ is entirely due to the granular stress, and the fluid flow and stress, while important above the bed, are irrelevant to determining the creep motion observed deep into the bed, where $\phi_g > 0.45$.

B. Suspension regime

We now focus on the observed flow profile in the suspension regime which develops clearly for f/f_c above 1.33. As discussed in Section IV B in interpreting the rise of shear stress with f, the entrainment of the grains can lead to an effectively higher viscosity of the fluid. We use the Krieger and Dougherty form [19] used to model the viscosity of a suspension containing solids in a Newtonian fluid as a function of their volume fraction,

$$\eta(\phi_g) = \eta_0(1 - \frac{\phi_g}{\phi_m})^{-B\phi_m}, \tag{2}$$

where, $B = 2.5$ is the Einstein coefficient, and ϕ_m is the maximum packing of the solid phase where viscosity diverges. This form reduces to the linear relation derived by Albert Einstein in the dilute limit $\phi_g \to 0$ with $\eta_0 = \nu$. Although this form was initially proposed for neutrally buoyant particles, it has been used even when this condition is not met. In

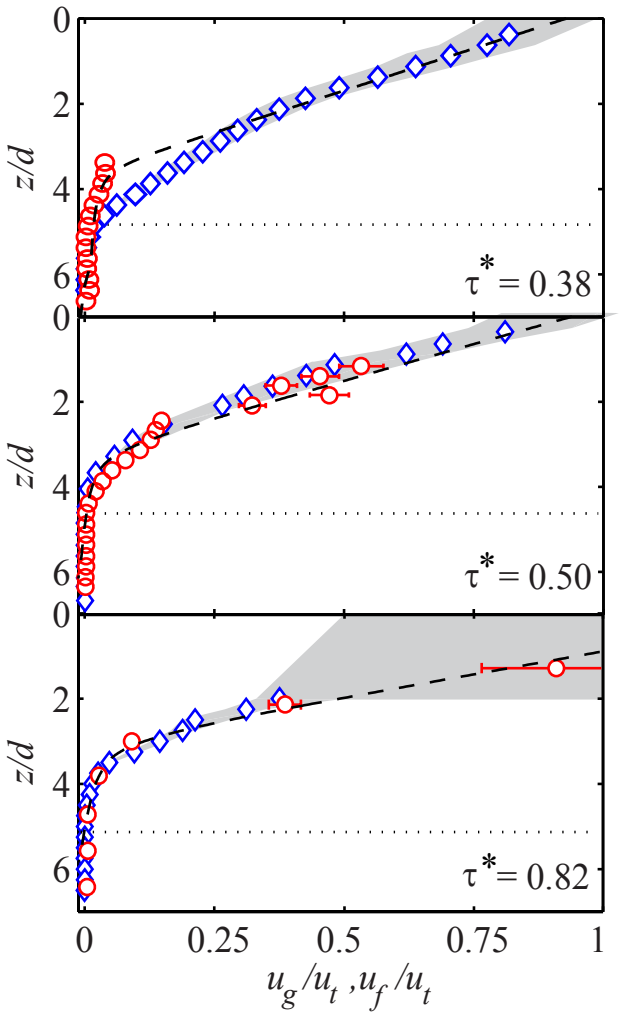


FIG. 8. (a-c) The grain velocity $u_g(z)$ (○) and fluid velocity $u_f(z)$ (◇) plotted using Eq. 3 for $\tau^* = 0.49, 50$, and 0.82. The dashed line (- - -) corresponds to calculating the velocity profile u_f using Equation 3 and can be seen to describe the flow when the particles are pulled into suspension, and when u_f and u_g are approximately the same. The dotted horizontal lines $(\cdots)$ correspond to the depth above which $\phi_g < 0.45$. The area shaded in gray correspond to the error in determing the velocities.

particular, the Krieger and Dougherty form has been found to be consistent with rheology measurements in case of dilute suspension of glass beads in viscous fluids [23]. From our experimental measurements we assume $\phi_m \approx 0.6$, and focus on the regime where $u_f \approx u_g$ to neglect the relative motion of the grains and the fluid. Then,

$$u_g(z) \approx u_f(z) = \frac{1}{\eta_0} \int_0^z (1 - \frac{\phi_g(z)}{\phi_m})^{B\phi_m} \, \mathrm{d}z \, . \tag{3}$$

We plot the experimental data along with $u_g(z)$ from Eq. 3 for $f/f_c = 1.26$, 1.33, and 1.43 in Fig. 8. Good agreement is observed provided $u_g \approx u_f$, $f/f_c \geq 1.33$ and assuming $\eta_0 = 1.5\nu$. This higher value of η_0 appears to be consistent with the higher effective drag in the transitional regime compared to the viscous regime. One can estimate an effective viscosity 1.9 ± 0.3 Pa s by dividing the measured τ in case of the flat substrate by $\dot{\gamma}$. In the case where significant slip exists between the granular phase and the fluid as in $\tau^* = 0.38$ shown in Fig. 8(a), this approximation does not capture u_g or u_f, but rather goes in between the two across the bed-fluid interface.

One can understand the range over which the Krieger and Dougherty form captures the observed flow field by considering the time scale over which a grain settles over the scale of its diameter and the advection time scale over which the grains move past each other due to the shear present in the system. By balancing the gravitational force with drag force acting on the grain, we have the time scale associated with gravity as a $t_g = 18\nu/(\rho_g - \rho_f)gd$. Then, assuming the advection time scale $t_a \approx 1/\dot{\gamma}$, we have the ratio of the time scales $t_a/t_g \approx (\rho_g - \rho_f)gd/18\nu\dot{\gamma}$. Substituting the values corresponding to the physical constants and the shear rate corresponding to our experiments, we find t_a/t_g is of order 0.1 in the region above the granular surface above the onset of granular transport, and decreases further as shear rate is increased. Thus, this form appears to describe the data in regions where the volume fraction of the grains is sufficiently small.

VI. CONCLUSIONS

In conclusion, we have developed an understanding of the flow profiles observed in a granular bed sheared by a fluid flow with experiments that enable depth-resolved flux measurements. By measuring the shear stress with two different techniques using torque and direct particle tracking, we find that the flow is in the transitional regime at onset of granular transport. The experiments are performed with grains and a fluid with density contrast which is similar to natural sand. However, in making a connection to sediment transport in rivers and streams, it should be noted that the fluid used for index matching is more viscous than water. This implies that the relevant flow in rivers and streams for similar size and density grains will be even further into the transitional regime. Nonetheless, it is possible that these results apply to finer grains in a lower viscosity fluid with appropriate scaling.

From these measurements, we find that the shear stress required to transport grains, increases rapidly as grains are suspended by the shearing fluid above the onset of transport. From the applied shear stress and the Krieger-Dougherty model for the effective viscosity, we are able to describe the overall form of the velocity profiles in the rapidly moving suspension regime. Further, in the slow flowing dense granular regime, we show that mean velocity of the granular phase decays exponentially into the bed with a decay constant which is described by a nonlocal rheology model of granular flow that neglects fluid stress. Although the shear due to the fluid flow above is the overall reason for the granular flow, the presence of the fluid is found to be unimportant to the dynamics deep inside the slow dense granular flow regime.

Finally, we note that while we have measured the velocity of the grains moving at the surface of the bed and described the subsequent decay of granular flow into the bed, we have not described the functional increase of the grain velocity nor the flux as a function of shear stress in the bed-load regime. We hope that our report will stimulate further research in this direction.

ACKNOWLEDGMENTS

We thank Ken Kamrin for stimulating discussions, and Ashish Orpe and Andreea Panaitescu for help with experiments. This material is based upon work supported by the U.S. Department of Energy Office of Science, Office of Basic Energy Sciences program under DE-FG02-13ER16401, and the National Science Foundation Grant # CBET 1335928.

---

[1] R. A. Bagnold, "The nature of saltation and of bed-load transport in water," Proceedings of the Royal Society of London A: Mathematical, Physical and Engineering Sciences **332**, 473 (1973).

[2] L. C. Van Rijn, "Sediment transport, part I: Bed load transport," Journal of Hydraulic Engineering **110**, 1431 (1984).

[3] J. M. Buffington and D. R. Montgomery, "A systematic analysis of eight decades of incipient motion studies, with special reference to gravel-bedded rivers," Water Resource Research **33**, 1993 (1997).

[4] E. Meyer-Peter and R. Müller, "Formulas for bed-load transport," Proceedings of the 2nd Meeting, International Association for Hydraulic Structures Research, Stockholm, Sweden **2**, 39 (1948).

[5] F. Charru, H. Mouilleron, and O. Eiff, "Erosion and deposition of particles on a bed sheared by a viscous flow," Journal of Fluid Mechanics **519**, 55 (2004).

[6] A. E. Lobkovsky, A. V. Orpe, R. Molloy, A. Kudrolli, and D. H. Rothman, "Erosion of a granular bed driven by laminar fluid flow," Journal of Fluid Mechanics **605**, 47 (2008).

[7] A. Hong, M. Tao, and A. Kudrolli, "Onset of erosion of a granular bed in a channel driven by fluid flow," Physics of Fluids **27**, 013301 (2015).

[8] J. Derksen and R. Larsen, "Drag and lift forces on random assemblies of wall-attached spheres in low-reynolds-number shear flow," Journal of Fluid Mechanics **673**, 548 (2011).

[9] C. Chan-Braun, M. García-Villalba, and M. Uhlmann, "High performance computing in science and engineering '10," (Springer, Berlin, Heidelberg, 2011) Chap. Direct Numerical Simulation of Sediment Transport in Turbulent Open Channel Flow, p. 295.

[10] O. Durán, B. Andreotti, and P. Claudin, "Numerical simulation of turbulent sediment transport, from bed load to saltation," Physics of Fluids **24**, 103306 (2012).

[11] A. H. Clark, M. D. Shattuck, N. T. Ouellette, and C. S. O'Hern, "Onset and cessation of motion in hydrodynamically sheared granular beds," Physical Review E **92**, 042202 (2015).

[12] R. Maurin, J. Chauchat, B. Chareyre, and P. Frey, "A minimal coupled fluid-discrete element model for bedload transport," Physics of Fluids **27**, 113302 (2015).

[13] H. Mouilleron, F. Charru, and O. Eiff, "Inside the moving layer of a sheared granular bed," Journal of Fluid Mechanics **628**, 229 (2009).

[14] P. Aussillous, J. Chauchat, M. Pailha, M. Médale, and É. Guazzelli, "Investigation of the mobile granular layer in bedload transport by laminar shearing flows," Journal of Fluid Mechanics **736**, 594 (2013).

[15] M. Houssais, C. P. Ortiz, D. J. Durian, and D. J. Jerolmack, "Onset of sediment transport is a continuous transition driven by fluid shear and granular creep," Nature Communications **6**, 6527 (2015).

[16] A. Armanini, H. Capart, L. Fraccarollo, and M. Larcher, "Rheological stratification in experimental free-surface flows of granular-liquid mixtures," Journal of Fluid Mechanics **532**, 269 (2005).

[17] C. Ancey, T. Böhm, M. Jodeau, and P. Frey, "Statistical description of sediment transport experiments," Physical Review E **74**, 011302 (2006).

[18] F. Boyer, É. Guazzelli, and O. Pouliquen, "Unifying suspension and granular rheology," Physical Review Letters **107**, 188301 (2011).

[19] I. M. Krieger and T. J.. Dougherty, "A mechanism for non-newtonian flow in suspensions of rigid spheres," Transactions of the Society of Rheology **3**, 137 (1959).

[20] S. Siavoshi, A. V. Orpe, and A. Kudrolli, "Friction of a slider on a granular layer: Nonmonotonic thickness dependence and effect of boundary conditions," Physical Review E **73**, 010301 (2006).

[21] A. Panaitescu, K. Anki Reddy, and A. Kudrolli, "Nucleation and crystal growth in sheared granular packings sphere packings," Physical Review Letters **108**, 108001 (2012).

[22] A. Goharzadeh, A. Khalili, and B. B. Jorgensen, "Transition layer thickness at a fluid-porous interface," Physics of Fluids **17**, 057102 (2005).

[23] S. Mueller, E. W. Llewellin, and H. M. Mader, "The rheology of suspensions of solid particles," Proceedings of the Royal Society A: Mathematical, Physical and Engineering Sciences **466**, 1201 (2010).

[24] D. Henann and K. Kamrin, "A predictive, size-dependent continuum model for dense granular flows," Proceedings of the National Academy of Sciences **110**, 6730 (2013).

[25] D. M Mueth, G. F. Debregeas, G. S. Karczmar, P. J. Eng, S. R. Nagel, and H. M. Jaeger, "Signatures of granular microstructure in dense shear flows," Nature **406**, 385 (2000).

[26] T. S. Komatsu, S. Inagaki, N. Nakagawa, and S. Nasuno, "Creep motion in a granular pile exhibiting steady surface flow," Physical Review Letters **87**, 1757 (2001).